Biofouling

The Journal of Bioadhesion and Biofilm Research

ISSN: 0892-7014 (Print) 1029-2454 (Online) Journal homepage: http://www.tandfonline.com/loi/gbif20

Modeling and analysis of hydrodynamic and physico-chemical effects in bacterial deposition on surfaces

Eli Margalit, Alexander Leshansky & Viatcheslav Freger

To cite this article: Eli Margalit, Alexander Leshansky & Viatcheslav Freger (2013) Modeling and analysis of hydrodynamic and physico-chemical effects in bacterial deposition on surfaces, Biofouling, 29:8, 977-989, DOI: 10.1080/08927014.2013.823483

To link to this article: http://dx.doi.org/10.1080/08927014.2013.823483

Biofouling, 2013
Vol. 29, No. 8, 977–989, http://dx.doi.org/10.1080/08927014.2013.823483

Taylor & Francis
Taylor & Francis Group

Modeling and analysis of hydrodynamic and physico-chemical effects in bacterial deposition on surfaces

Eli Margalit[a], Alexander Leshansky[b] and Viatcheslav Freger[b]*

[a]*Faculty of Engineering Sciences, Unit of Environmental Engineering, Ben-Gurion University of the Negev, Beer-Sheva, Israel;* [b]*Wolfson Department of Chemical Engineering, Technion – Israel Institutes of Technology, Haifa, Israel*

(*Received 26 January 2013; final version received 13 June 2013*)

The parallel-plate flow chamber (PFC) is often used for characterizing the propensity of microorganisms to attachment to surfaces. The model presented quantitatively analyzes the complex interplay of diffusion, convection, inertial lift, buoyancy, and surface forces in the PFC, which make it difficult to separate the surface- and microorganism-specific effects from the hydrodynamics. An empirical dimensionless factor K entering the boundary condition expresses enhancement of adhesion diffusion of microorganisms across a thin fluid layer adjacent to the surface by adhesion forces. The model examines the role of various factors (eg shear rate, size of bacterium, and strength of adhesion) on the rate of bacterial deposition. Using no adjustable parameter for strongly adhesive surfaces and K as the only adjustable parameter for repulsive or weakly adhesive surfaces, the model explains the observed decrease in deposition flux at high flow rates and compares reasonably with reported experimental results. The results suggest that the fitted value of K may be used for 'rating' the propensity of bacteria to deposit on surfaces and separating this from hydrodynamic effects.

Keywords: bacterial deposition rate; modeling; inertial lift; buoyancy; antifouling surface rating

Introduction

Bacteria and other microorganisms attach to substrata as an initial colonization step in the formation of biofilms and the biofouling of surfaces and the pore spaces of porous media (Costerton et al. 1995). Biofilms occur in many fields of industrial and medical applications; in some cases their formation is beneficial, eg in bioremediation processes resulting in the degradation of hazardous chemicals in the soil or in the treatment of wastewater or off-gas (Hori & Matsumoto 2010). However, in most cases biofilms are undesired and cause damage or reduced performance, eg on ships' hulls, the surface of heat exchangers, food packaging materials, medical devices, implants, vascular grafts, and membrane filtration systems.

The formation of a biofilm proceeds as a succession of several phenomena (Palmer & White 1997), namely; (1) surface conditioning, ie the adsorption of a variety of biomolecules that promote the adhesion of microorganisms; (2) the transport of individual microorganisms into close proximity with the surface; (3) the reversible or irreversible adhesion of the cell to the surface; (4) the formation of microcolonies and biofilms *via* cell growth and division, accompanied by phenotype and genotype changes; (5) the proliferation of the biofilm *via* cell redispersal for colonization of new areas (Bjarnsholt 2011). The present study focuses on to the first three stages, collectively referred to as bacterial or, more generally, as microorganism deposition, which precede and are critical for the subsequent formation of a biofilm.

The models of bacterial deposition proposed in the literature have been based on the convection-diffusion-migration (CDM) equations of mass transfer (Elimelech et al. 1995). The inclusion of migration accounts for the effect of external forces and the interaction of the bacterium with the substratum. One external force is gravity, which was found to have a substantial effect on deposition of bacteria and micron-sized particles (Chen et al. 2009; Li, Busscher, Norde, et al. 2011; Li, Busscher, van der Mei, et al. 2011). Other important forces include those acting near the surface of the substratum that are mediated by a variety of interactions including Lifshitz–van der Waals, electrostatic, hydrophobic, and hydration forces, and whose role on the deposition of microorganisms has been modeled extensively (Adamczyk & Weronski 1999; de Kerchove et al. 2007).

The conventional CDM approach was applied successfully to model the role of adhesion forces in bacterial deposition for the radial stagnant point setup (de Kerchove et al. 2007). In this setup, the flow is normal to the surface and radially symmetrical at one particular location, thus the problem becomes one-dimensional and modeling, including surface forces, is fairly straightforward. However, such a situation is rare in reality and cases when the flow is tangential are far more common.

*Corresponding author. Email: vfreger@tx.technion.ac.il

A typical tangential flow setup is the parallel-plate flow chamber (PFC), a popular research tool (Roosjen et al. 2005; Chen et al. 2009; Wang et al. 2011). If gravitational sedimentation is neglected and adhesion is described simply through a perfect sink boundary condition, the problem is analogous to the classical Graetz problem of forced convective heat transfer in a channel geometry. This yields a well-known simple analytical solution, the Levich-Smoluchowski approximation (Elimelech 1994) also known as Lévêque's solution in heat transfer. This solution predicts that the deposition rate should always increase with flow velocity or, equivalently, shear rate at the wall. It is to be emphasized that the addition of external forces, eg gravity, or replacing the perfect sink conditions with a distributed adhesion force field, is not supposed to alter this general trend.

Surprisingly, the results of deposition experiments in PFCs often show an opposite trend, deposition rate decreasing with increasing fluid velocity (Bakker et al. 2002; Roosjen et al. 2005). This suggests that convection is overridden by some hydrodynamic force that progressively hinders deposition when the flow rate increases, which is unaccounted for and not included in published models of bacterial deposition. Boks et al. (2008) suggested that such a force must be present, but they did not specify any physical mechanism. Recent results (Li, Busscher, Norde, et al. 2011; Li, Busscher, van der Mei, et al. 2011) suggested another possibility, namely that strong sedimentation combined with the drag of bacteria deposited along the surface might explain the observed dependence without invoking any extra force. However, as will be discussed later in the paper, this mechanism may not be sufficiently general. The present study attempts to address this problem at a quantitative level and provide an adequate correction to the CDM modeling framework.

An additional motivation for the study arises from the need to quantitatively separate hydrodynamics from adhesion forces. This separation will be beneficial, for instance, for comparing the propensities or resistances of surfaces to biofouling, as the rate of microorganism deposition on a surface is widely used as an indicator. In the absence of adequate models, the comparison of different surfaces based purely on deposition rates may be obscured by hydrodynamics, especially when the setups and deposition conditions are not identical. The present study attempts to address this.

The proposed correction essentially accounts for the hydrodynamic force acting in the direction transverse to the flow. Such forces are usually referred to as 'lift' and their origin is hydrodynamic yet, unlike convective drag, comes from fluid inertia rather than viscous forces. The seminal paper of Segre and Silberberg (1962) reported that particles suspended in a Poiseuille flow in a pipe experienced a position-dependent radial force, and correctly attributed it to the inertia of the fluid. Numerous experimental and theoretical studies followed (Brenner 1961; Saffman 1965; Goldman et al. 1967), which were later extended to more general cases including different flow regimes and non-neutrally buoyant particles (Ho & Leal 1974; Vasseur & Cox 1976; Cox & Hsu 1977; Asmolov 1999; Yahiaoui & Feuillebois 2010). These results have been used extensively in various fields, such as microfiltration (Altena & Belfort 1984), particle deposition (Song & Elimelech 1995; Maniero & Canu 2006; Maniero & Canu 2007), and microfluidics (Di Carlo 2009), yet have found little use in studies of bacterial deposition in the context of biofouling. Hoek et al. (2008) included a lift force in their analysis of microorganism deposition on reverse osmosis membranes using, essentially, a simplified Lagrangian approach, which considered the drag of a single microorganism by all forces against permeation drag. The present work is an attempt to use an alternative Eulerian approach to construct a practically useful model that would describe collective deposition of microorganisms on different surfaces at a chosen location. Such an improved model, of minimal complexity yet capturing most essential physical effects including surface-specific adhesion forces, will be shown to compare reasonably well with experimental results.

Theoretical model

The model considers a plain Poiseuille flow of a dilute dispersion of non-motile bacteria, viewed here as Brownian spherical particles, in a channel between two parallel walls, a common configuration in bacterial deposition experiments (van Loosdrecht et al. 1989; Roosjen et al. 2005; Boks et al. 2008; Hori & Matsumoto 2010). An approximation adequate for most experiments is that the bacterial dispersion is sufficiently dilute to neglect hydrodynamic and physico-chemical interactions between bacteria. Figure 1 depicts the flow channel geometry, where $H=2b$ is the channel height, h is the distance between the center of gravity of the bacterium and the bottom wall, and a is the radius of the bacterium. The fluid velocity components U_x and U_y and wall shear rate σ are

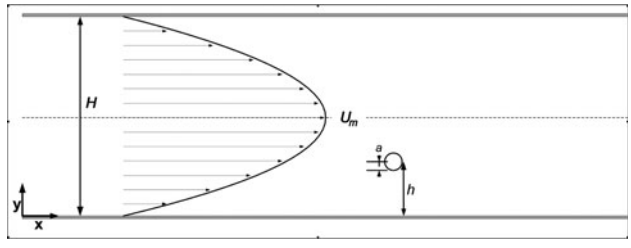

Figure 1. Schematic 2D representation of the geometry of the flow channel and spherical particle.

assumed to follow the fully developed Poiseuille flow (Figure 1), as follows:

$$U_x = \frac{3}{2}U_m\left[1-\left(\frac{H-2y}{H}\right)^2\right], U_y = 0 \qquad (1a)$$

$$\sigma = \left.\frac{dU_x}{dy}\right|_{y=0} = -\left.\frac{dU_x}{dy}\right|_{y=H} = \frac{6U_m}{H} \qquad (1b)$$

where U_m is the mean flow velocity. The velocity profile given by Equation 1a is not accurate for the undeveloped flow region at distances less than $\sim 0.05HRe$ from the entrance, where $Re = HU_m/v$ is the channel Reynolds number with v being the kinematic viscosity (Levich 1962). For a typical range of shear rates $1–10^3\,s^{-1}$ and $H \sim 1$ mm this region never extends beyond a few millimeters from the entrance, and the associated error is therefore not large, unless the channel is very short.

Neglecting the finite width of the channel, the governing two-dimensional CDM equation is written here as:

$$\nabla \cdot \boldsymbol{J} = \nabla \cdot \left[-D\nabla C + \frac{DC}{kT}\boldsymbol{F} + (\boldsymbol{U}+\boldsymbol{U}')C\right] = 0 \qquad (2)$$

where J is the local flux, C is the concentration of bacteria, F the total force acting on the bacterium, U the undisturbed fluid velocity given by Equation 1a, and U' is the slip velocity of the bacterium relative to the fluid. Far from the wall the bacterium diffusivity (D) is given by the Stokes–Einstein relation:

$$D = D_0 = \frac{k_B T}{6\pi\mu a} \qquad (3)$$

Near the wall D decreases below its bulk value (D_0) and becomes anisotropic and dependent on the particle-to-wall distance (h) due to hydrodynamic interactions with the wall. Similarly, the particle motion along the wall is hindered relative to the fluid by interaction with the wall. Appropriate near-wall corrections as a function of h are available for tangential and normal components of D and U' (Elimelech et al. 1995).

The forces generally included in F and considered in this study are surface adhesion forces, buoyancy (gravity) and lift. It must be emphasized that lift fundamentally differs for the other two in that it is a hydrodynamic force and thus it is not conservative, ie has no field or potential. It may also be coupled to the other forces, eg buoyancy (Hogg 1994). Nevertheless, for a given fluid velocity profile, as in a PFC, the lift force often depends only on the coordinate y, which allows it to be formally viewed as a quasi-conservative force and for a corresponding quasi-potential field to be defined (see below). To do so, lift must also be effectively decoupled from other forces, buoyancy in particular. As discussed by Hogg (1994), for vertically aligned channels lift and buoyancy are unconditionally decoupled, however, in a horizontal channel coupling is negligible only provided $\left(\frac{2}{9}\frac{a^2\Delta\rho g}{\mu U_m}\right)^2 Re \ll 1$, where $\Delta\rho$ is the difference in the densities of the particles and the fluid, and g is the gravitational acceleration (Hogg 1994). The typical values of parameters relevant to the present case ($a \sim 10^{-6}$ m, $\Delta\rho \sim 10^2\,kg\,m^{-3}$, $\mu = 10^{-3}$ Pa s, $U_m \sim 10^{-3}\,m\,s^{-1}$ and $Re \sim 1$) set the upper bound of $\left(\frac{2}{9}\frac{a^2\Delta\rho g}{\mu U_m}\right)^2 Re$ to $\sim 10^{-6}$ which suggests that the lift force may indeed be treated as a quasi-conservative additive force uncoupled from buoyancy.

Assuming the chamber is horizontal, as typically required for microscopic observation of deposition, only the y components of the buoyancy and lift forces, F_G and F_L respectively, are non-zero. They are expressed as:

$$F_G = -\frac{\pi}{6}a^3 g\Delta\rho \qquad (4)$$

$$F_L = \frac{1}{36}\rho\sigma^2 a^4 G(S) \qquad (5)$$

where $S = h/H$ and the dimensionless function GS represents the variation of F_L across the channel in a Poiseuille flow. Both F_G and F_L depend strongly on the size of the bacterial cells. While F_G is independent of the flow rate and is of the order of 10^{-16}–10^{-15} N, F_L depends strongly on the rate of flow and, as σ increases from $\sim 10^0$ to $>10^3\,s^{-1}$, as in this study, the lift force near the wall varies from $\sim 10^{-21}$ to 10^{-14} N, eventually overwhelming F_G.

The function $G(S)$ is anti-symmetric with respect to the channel center-plane ($S = 0.5$). The dependence of F_L on S has been evaluated analytically and numerically for different cases (Goldman et al. 1967; Ho & Leal 1974; Cox & Hsu 1977; Asmolov 1999; Matas et al. 2004). The trends reported are similar, however different assumptions and ranges of applicability lead to substantial differences near the wall. To examine the significance of these differences, this study employed numerical results presented by Ho and Leal (1974) and an analytical expression by Cox and Hsu (1977). To facilitate their use in simulations, the numerical data (Ho & Leal 1974) were fitted to the regression given in Equation 6a, inherently anti-symmetric with respect to $S = 0.5$:

$$G(S) = \frac{A}{(B+S)^2} - \frac{A}{(1-B-S)^2} + C(S-0.5) - D(S-0.5)^3 + E(S-0.5)^5 \qquad (6a)$$

The fit yielded $A = 1.357$, $B = 0.05836$, $C = 125.5$, $D = 1550$, $E = 8835$ with an $r^2 = 0.9992$ (Figure 2). The analytical result of Cox and Hsu (1977) is also depicted (Figure 2) and may be expressed as follows:

$$G(S) = -\frac{5\pi}{12}(2S-1)(73|2S-1|-51) \qquad (6b)$$

Although the absolute value of $G(S)$ is largest near the wall, it is of substantial magnitude throughout the channel and, thereby, it cannot be ignored in Equation 2 anywhere across the chamber. For both equations the two zeros of $G(S)$ at $S \sim 0.2$ and $S \sim 0.8$ correspond to stable equilibrium locations, where the particles tend to accumulate. The most notable difference between Equations 6a and 6b is the divergence of $G(S)$ near the wall, ie at $S = 0$, found by Ho and Leal (1974). Yet, their solution is valid for small Re and, strictly speaking, is inaccurate in the near-wall region where $G(S)$ increases sharply. However, logically even when a particle touches the bottom wall, S cannot be smaller than $S_{min} = a/H \sim 10^{-3}$ thus $G(S)$ remains finite and the solution of Equation 2 is not divergent.

The analysis by Cox and Hsu (1977) removes the assumption of small Re and yields an improved solution for F_L in the near-wall region, valid to within a few particle radii from the wall. This solution extrapolates to a finite value even at $S = 0$, and is confirmed by more accurate later results (Cherukat & McLaughlin 1994; Asmolov 1999; Yahiaoui & Feuillebois 2010). Notably, Equation 6b which is a simple analytical result is essentially not different from the more elaborate analytical solution of Cherukat and McLaughlin (1994). It also closely agrees with thorough recent computations by Yahiaoui and Feuillebois (2010) that apply down to distances from the wall well below the particle radius (a).

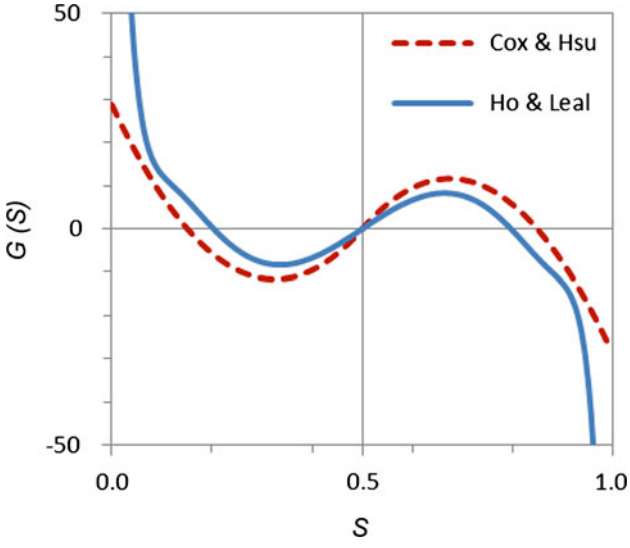

Figure 2. The dimensionless function $G(S)$ given by Equation 6a and 6b.

In contrast to F_L, the adhesion force (F_a) is truly negligible everywhere except for a very short range near the wall, even if the force is strong enough to produce irreversible deposition. F_a typically extends to no more than 1 μm, ie no more than the diameter of a bacterial cell from the wall (Adamczyk & Weronski 1999). In general, F_a involves electrostatic (double layer), dispersive, hydrophobic, solvation and other interactions, and its spatial variation near the wall depends strongly on the chemical nature, surface charge and hydration of the specific bacteria and surface as well as the pH and salinity of the solution (Elimelech 1994; Yiantsios & Karabelas 2003; Hoek & Agarwal 2006). It is also highly sensitive to, for example contamination, the presence of a conditioning film, an adsorbed layer, and surface roughness. These factors may also vary widely among the species of microorganism and the surfaces upon which they deposit, as well as being influenced by, for example, the growth phase, habitat and environmental conditions (Roosjen et al. 2005; Busscher & van der Mei 2006; Boks et al. 2008; Ploux et al. 2010). It is unrealistic to expect that the physical parameters pertaining to such a variety of interactions may ever be accurately measured for each type of interaction involved in real-world scenarios.

In actuality the situation is even more complicated, given the rapid variations in the diffusivity components D_x and D_y and the slip velocity U' as well as steep variations in the lift force near the surface at distances commensurate with a. It is then not surprising that no meaningful quantitative physical 'rating' has been proposed of surfaces for the propensity of bacterial deposition, deducible from deposition experiments and separate from hydrodynamic effects. Towards this goal, it is proposed here to redefine the problem in a simplified way and seek an overall 'rating' of physical interaction with the surface rather that accurately modeling all molecular and hydrodynamic interactions at the closest proximity of the wall.

The approximate approach proposed here is as follows. In Equation 2 the adhesion force (F_a), slip velocity (U'), and the deviation of the particle diffusivity (D) from the bulk value (D_0) all decrease rapidly with distance from the wall. Therefore, as an approximation, they are ignored in Equation 2 everywhere beyond a thin region, adjacent to the wall, of a thickness a' commensurate with particle radius a. It should be noted that in this way U' is dropped in Equation 2, but still implicitly affects the lift force. Within this region the effect of the adhesion force F_a enters through the following ad hoc boundary conditions:

$$\boldsymbol{J} = \left[-D_0\nabla C + \frac{D_0 C}{kT}\boldsymbol{F} + \boldsymbol{U}C\right]_{y=a'} = K\frac{D_0}{a'}[C_s - C(y=a')]\boldsymbol{r} \quad (7)$$

where r is the unit vector normal to the wall, C_s is the solution concentration in equilibrium with the surface, and K is a dimensionless fitting kinetic parameter. Equation 7 states basically that at $y=a'$ the deposition rate given by Equation 2, that includes in F only gravity and lift, is matched with an expression at the right borrowed from the kinetics of heterogeneous reactions. The concentration C_s conveniently gauges the state of bacterial adsorption on the surface and is what would hypothetically occur in a stagnant solution, if the solution and surface in a given state came in thermodynamic equilibrium. This definition of C_s assumes the solution is at the same height as the surface, thereby the force of gravity does not affect the equilibrium. If the surface is clean initially, the rate of deposition will remain approximately constant as long as $C(a') \gg C_s$, ie far from saturation. This linear regime of initial deposition was considered in most reported experiments using a PFC, in which case $C_s=0$ is a good approximation throughout the experiment. The present paper focuses mainly on this regime.

The parameter K is proposed here to serve as a 'rating' of the propensity of a specific surface to the deposition of specific microorganisms. K combines all the different interactions near the surface, at distances $h \sim a$ from the wall, in just one parameter, specific for the given surface, microorganism and fluid medium. Supposedly, this parameter is less dependent on hydrodynamics than the rate of deposition itself. Neglect of slip and variations of diffusivity near the wall will bias the value of K but will not change the general trend. Given the crude nature of the model, this simplification might be acceptable.

The factor D_0/a' at the right of Equation 7 gauges the rate of deposition against the rate of bulk diffusion across a fluid layer of thickness a', thereby K is dimensionless. It can be seen that $K=\infty$ corresponds to a perfect sink condition, ie $C=C_s=0$ at $y=a'$, regardless of the actual state of the surface. The ideal sink condition on the wall ($C=0$, $a'=0$) has been used often in theoretical deposition models, especially when adhesion forces are explicitly included (Adamczyk & Weronski 1999). In contrast, when $K=0$ no deposition occurs, ie the surface is ideally repulsive to microorganisms, and $K \sim 1$ corresponds to the case when there is a weak adhesion or repulsion.

Equation 7 with $C_s=0$ is similar to the boundary condition proposed by Yiantsios and Karabelas (2003) for deposition of solid particles on different surfaces. They introduced a parameter, dimensionless 'attachment coefficient' analogous to K that corresponds to $a'=a$, yet the expressions at the left and right sides of Equation 7 were matched close to the wall, at $y \leqslant 0.01a \leqslant\leqslant$ rather than at $y=a$. The meaning of 'attachment coefficient' was therefore slightly different from the present case, as it was assumed to incorporate only adhesion forces over the range of just a few nm. However, this range grossly underestimates the range of adhesion forces, which is substantially longer for micron-sized particles and microorganisms. Conversely, Yiantsios and Karabelas (2003) included in their equations near-wall hydrodynamic corrections to the diffusivity and slip velocity, which are ignored in Equations 2 and 7. It then appears that in either case near-wall hydrodynamic corrections are incorporated into adhesion forces at distances of $y \sim a \sim 1$ μm with some inevitable bias. However, the use of a constant bulk diffusivity and zero slip velocity in Equations 2 and 7 simplifies the equations and numerical solution in the present case, as compared to more elaborate model of Yiantsios and Karabelas (2003).

Numerical solution

Two-dimensional Equation 2 was solved using COMSOL Metaphysics 4.0a software (COMSOL, Comsol Inc., Burlington, MA, USA; www.comsol.com). The standard routine 'transport of diluted species' was used, which includes migration through an appropriately defined mobility and potential. The buoyancy and lift forces were thus included through the potential of a gravity field in liquid and the pseudo-potential obtained by integration of Equation 5, respectively. The Einstein formula was used to relate mobility to D.

The boundary condition for the bottom and top plates were given by Equation 7 with $C_s=0$ and $a'=2a$. The latter was chosen arbitrarily to narrowly enclose the range of adhesion forces (<1 μm). However, it was verified that the results were virtually independent of the particular choice of a', as long as it was of the order of a. When gravity was not included, calculations were performed only for the bottom half-channel using a symmetry condition at the channel centerline. The concentration was normalized to the concentration at the entrance $C(x=0)=C_0$, which was assumed to be constant.

The geometry of the PFC was chosen to match the one used in the experiments of Roosjen et al. (2005) and Boks et al. (2008). The channel height (H) was set to 0.75 mm and the length (L) to 175 mm. The finite mesh elements were rectangles with a length: width ratio (X:Y) of 100, which accounted for much steeper variation in concentration in the Y direction. The mesh size in the Y direction was further reduced near the wall to 0.5 μm per element. If not stated otherwise, the calculated flux on the boundary corresponded to the half-length of the channel. It was averaged using line integration over the 1 mm length bracketing the half-length point, which emulated microscopic observations in PFC experiments.

Results and discussion

The effect of flow rate on particle deposition

The primary goal of this study was to analyze numerically the effect of the lift force, as well as buoyancy, on the kinetics of bacterial deposition. As the lift force shows a strong dependence on the fluid velocities or, equivalently, wall shear rates, the simulations were performed for a wide range of wall shear rates from 4 to $\sim 1600\,s^{-1}$, corresponding approximately to the experiments of Roosjen et al. (2005) and Boks et al. (2008). Figure 3a shows the computed normalized deposition flux $j = J/C_0$, often called the deposition coefficient, at the half-length of the channel. Figure 3b and c show the variation in this parameter along the channel. To see explicitly the effect of buoyancy and lift on deposition, the numerical solutions are compared to the classical Smoluchowski–Levich (SL) approximation (Equation 8):

$$j = \frac{J}{C_0} = 1.12\left(\frac{\sigma D^2}{9x}\right)^{1/3} \tag{8}$$

The SL approximation is the analytical solution of Equation (2) in Poiseuille flow near a channel wall for the classical perfect-sink boundary condition, corresponding to $a' = 0$, $C(y=0) = 0$, $D = D_0$, $U' = 0$ and $F = 0$, ie without interaction with the wall, slip, lift, and gravity or any other external force (Levich 1962). The curve computed without lift and gravity ($F = 0$) virtually coincides with the SL solution, a small deviation at very low flow rates is due to a small drop in the bulk concentration along the channel. The three cases where lift was included in calculations correspond to the bottom ($F < 0$) and top ($F > 0$) walls of a horizontal channel and to no-gravity conditions ($F = 0$) that apply to neutrally buoyant particles or vertical walls.

Figure 3a shows unequivocally that the effect of buoyancy is important at small wall shear rates, while lift becomes increasingly dominant as the flow accelerates and the wall shear rate increases. This result could be anticipated considering the dependence on the flow rate embedded in Equations 4, 5, and 8. Indeed the sedimentation force, and hence the sedimentation flux driven by gravity, in Equation 4, is independent of the flow rate, while the SL solution predicts that the deposition flux by the diffusion-convection mechanism increases with fluid velocity as $U_m^{(2/3)}$. Conversely, Equation 5 indicates that the lift force, opposing deposition, is proportional to U_m^2, ie increases faster and eventually dominates as the flow velocity increases. Most notably, gravity changes the absolute deposition rate but not the trend, whereas the

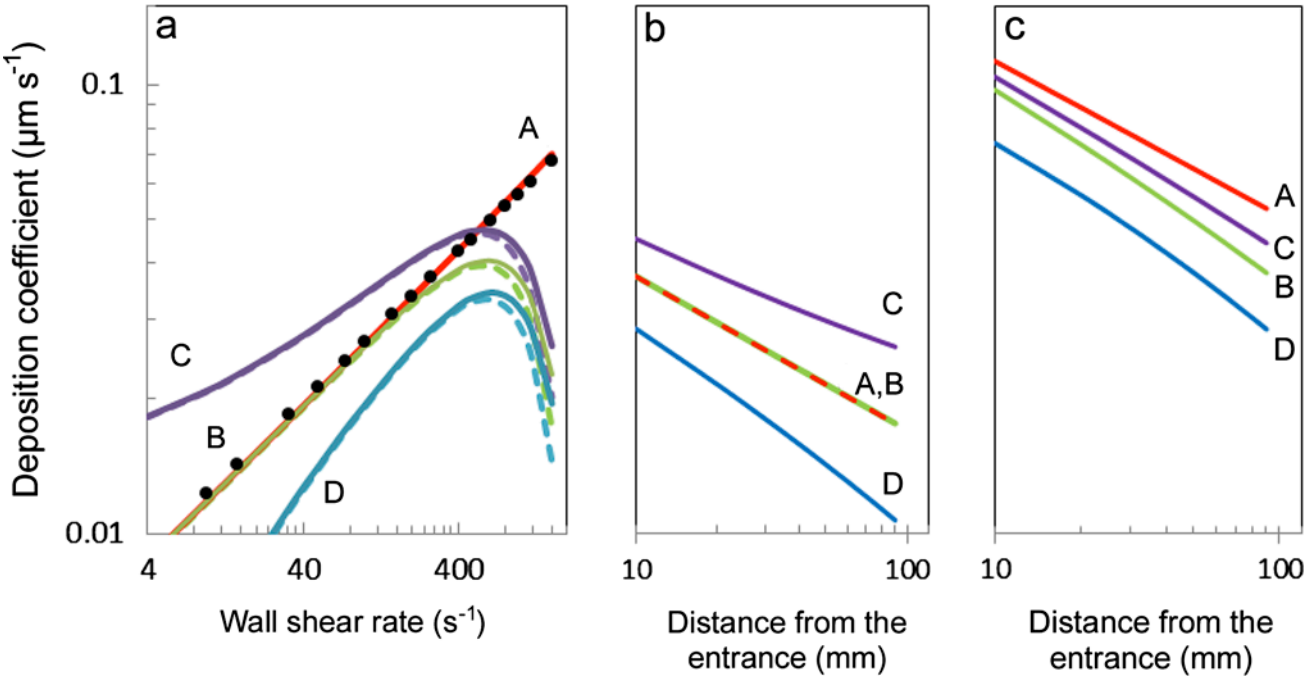

Figure 3. (a) Deposition coefficient as a function of wall shear rate calculated for bacteria of radius $a = 0.7\,\mu m$ in a horizontal parallel-plate flow channel of height 0.75 mm: no gravity or lift present ($F_L = F_G = 0$; line A), lift included without gravity ($F_G = 0$; line B), and both lift and gravity included for top (line C) or bottom (line D) surfaces. For lines B–D solid and dashed lines are obtained using, respectively: Equation 6b, Cox and Hsu (1977) or Equation 6a, Ho and Leal (1974) for F_G. Solid circles designate the SL solution Equation 8. The results represent local deposition flux at 87 mm from the entrance. (b) Variation in the deposition coefficient with the distance from the entrance for wall shear rate $33\,s^{-1}$; curves A–D correspond to the same cases as in (a). (c) Same as for (b) for a wall shear rate of $800\,s^{-1}$.

lift reverses the trend and the deposition rate begins to decrease above a certain flow rate. This trend, routinely observed in deposition experiments with various microorganisms, cannot be explained without considering a lift force, emphasizing its crucial role at high flow rates. This conclusion is independent of the particular expression used to calculate the lift force. The more accurate expression in Equation 6b from Cox and Hsu (1977) yields a weaker lift force (Figure 2) and hence predicts slightly higher deposition rates (by 20–30% at the highest shear rate used) compared to the approximation of Ho and Leal (1974) in Equation 6a. This difference may be considered inconsequential, given the typical uncertainties of measured deposition rates (see below).

The forces of gravity and lift also modify the variation of deposition rate along the channel, as shown in Figure 3b and c for a low and high shear rate, respectively. As before, the results are compared with the SL solution, Equation 2, which shows the characteristic linear slope of $-\frac{1}{3}$ on a double-log scale. At low shear rate, along with an increased deposition rate relative to SL, buoyancy makes the dependence more uniform for the bottom surface and the slope become less negative; the opposite takes place for the top surface. At high shear rates lift becomes a dominant factor, the deposition rate drops, and the slope becomes steeper relative to SL for all cases. It is seen that, in general, forces acting against deposition lead to a steeper variation of the deposition rate along the channel.

The effect of lift, calculated using the expression of Cox and Hsu (1977), is further illustrated in Figure 4 which shows the variation in the concentration profile across the channel with the flow rate near the bottom surface, with and without lift and/or gravity. The concentration gradient near the wall is related directly to the deposition rate in Equation 7. It can be seen that the gradient increases monotonically with the flow rate when the lift is neglected (Figure 4a). However, once the lift force is included (Figure 4b), it propels the bacteria away from the wall, yielding a trend reversal at high flow rates. This reduces the gradient and widens the region near the wall that is virtually depleted of particles (Figure 4b). The addition of gravity modifies the profiles somewhat, with more marked impacts at low shear rates (*cf.* Figure 4b and c).

The effect of particle size

Retrieval of the parameter K from deposition experiments using the proposed model requires accurate values for the size and density of the particles. The density of bacteria may vary quite markedly, between 1.04 and $1.13\,\mathrm{g\,cm^{-3}}$ (Chen et al. 2009), yet it mainly affects the buoyancy (sedimentation) in the low shear rate regime. The lift force is independent of the density of the particles and therefore uncertainty over bacterial density is not expected to affect the estimate of the deposition rate in the high-shear-rate regime. Deposition may also be affected by the motility of bacteria (Camesano & Logan 1998; Kerchove & Elimelech 2008; Haznedaroglu et al. 2010; Gutman et al. 2012) as well as their shape (nonsphericity), non-ideal rigidity, and deformability (van Oss 2006), yet these effects are complex and still relatively poorly understood. The present analysis will therefore be limited to the effect of size, that is apparently the most dominant and straightforward.

The diameter of a bacterium varies typically from 0.6 to 3.0 μm depending on the species and the environmental conditions (Wyatt & Phillips 1972; Palumbo et al. 1984). The variation is even larger, if eukaryotic microorganisms such as yeast cells or protozoa that may be as large as 12 μm (Prescott et al. 2002) are included. Since buoyancy and, especially, lift forces are strongly size-dependent (Equations 4 and 5), these variations may lead to profound differences in the rate of deposition that cannot be anticipated from the SL approximation. This point is illustrated in Figures 5 and 6 showing the deposition coefficient and concentration profiles calculated for neutrally buoyant particles of different radii under perfect sink boundary condition with the lift force included. It can be seen that minor changes in the particle size, within a factor 2.2 which is well within typical variations in the size of bacteria, may lead to a substantive change in the trends of deposition rate and its dependence on the hydrodynamic conditions.

While for $a = 0.5\,\mu\mathrm{m}$ in Figure 5 the deposition rate still increases monotonically when σ increases from 100 to $1000\,\mathrm{s^{-1}}$, for $a = 1.1\,\mu\mathrm{m}$ it reaches a maximum by $\sigma \approx 200\,\mathrm{s^{-1}}$ and then drops sharply to become nearly entirely eliminated at $\sigma > 1000\,\mathrm{s^{-1}}$, in contrast with the SL prediction. Figure 6a shows that the concentration and its gradient drop progressively in the vicinity of the wall, ie as their size increases bacteria are pushed away from the wall by the lift force. The addition of gravity modifies the profiles and flux for the top and bottom surfaces without changing the general trend (*cf.* Figure 6b and c).

The effects of surface interactions and comparison with experiments

The present model allows a simple insight into the effect of a particular surface on the rate of deposition for given hydrodynamics conditions and channel geometry through variation in K. Figure 7 shows a typical set of results obtained for neutrally buoyant particles. As K increases above 1, ie when adhesion forces become attractive, the results rapidly converge to the perfect sink solution and for $K = 10$ are virtually indistinguishable from those for $K = \infty$. However, below $K \sim 1$, when the surface switches

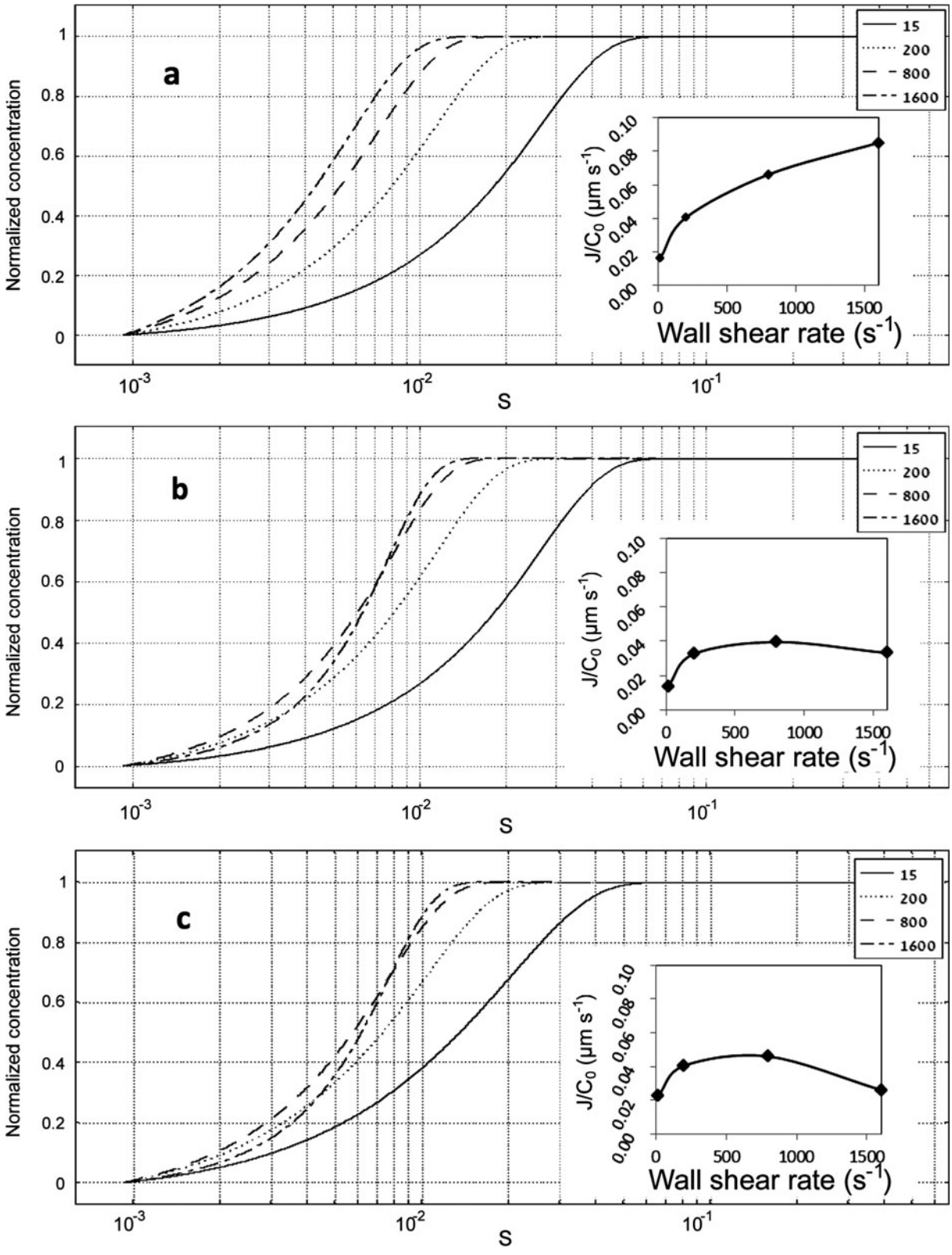

Figure 4. Concentration profiles normalized to feed concentration in the middle cross-section of the channel for shear rates 15, 200, 800, and 1600 s^{-1} *vs* $S=y/H$, the distance from the wall normalized to channel height: (a) neutrally buoyant particles without lift force, (b) neutrally buoyant particles with lift force included, and (c) particles of density 1.1 g cm^{-3} depositing on the bottom wall with lift force included. Particle radius is 0.7 μm. Channel height and length are 0.75 and 175 mm, respectively, wall shear rate of 800 s^{-1}.

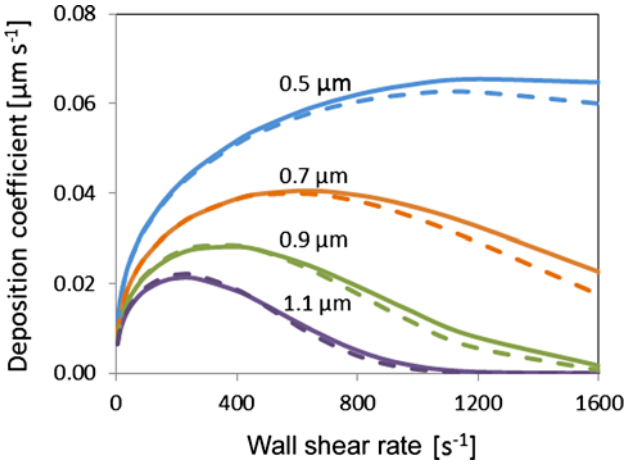

Figure 5. The deposition coefficient as a function of wall shear rate for neutrally buoyant spherical particles showing the effect of particle radius. The results are for the perfect-sink boundary condition at the bottom wall. Solid and dashed lines are obtained using, respectively: Equation 6b, Cox and Hsu (1977), or Equation 6a, Ho and Leal (1974).

from attractive to repulsive, the rate of deposition drops exponentially and is markedly affected by the nature of the surface. This is in good accord with the findings of Kalasin and Santore (2008) who observed approximately constant rates of deposition of charged particles on an attractive surface, which sharply crossed over to immeasurably low rates as the surface was gradually made repulsive. In addition, Figure 7 shows that the maximum rate of deposition steadily shifts to lower shear rates and the range of the decreasing trend widens as K decreases, ie as the surface becomes more repulsive. This is again in agreement with the results of Kalasin and Santore (2008), which would be predicted, since the lift force is independent of K whereas diffusion becomes slower as K decreases. The lift force begins to dominate the trend at lower shear rates, and at $K \sim 0.001$ it becomes decreasing in the entire analyzed range. It appears that, at this K, the near-surface transport resistance, assumed to be independent of shear rate in the present model, dominates over the bulk resistance up to shear rates where the bulk resistance is increased by the lift force.

The picture becomes more complex when buoyancy (sedimentation) is added along with the lift force. The trends observed in Figure 7 retain their main features, when particle deposition is reduced or enhanced by sedimentation, ie on the top and bottom surfaces, (Figure 8a and b, respectively). For the bottom surface the trend retains a maximum, down to the lowest values of K used, while for the top surface the maximum disappears and the trend becomes decreasing in the whole range of shear rates analyzed at $K \sim 0.03$, ie for a less repulsive surface than in Figure 7. The effect of K on the trends observed apparently reflects the variations in the relative contributions of near-surface and bulk transport resistances in each case.

To illustrate how the model applies to real-world situations Figure 9 compares simulations performed under perfect sink boundary conditions ($K = \infty$) to the deposition rates obtained experimentally for top and bottom glass surfaces in a PFC cell for the bacterium *Staphylococcus epidermidis* ATCC 35983 (Boks et al. 2008). The simulation used the reported radius of the bacterium, $a = 0.9\,\mu m$ and a typical density of $1.1\,g\,cm^{-3}$. The use of the perfect sink boundary is consistent with the observation that the attachment of this strain to glass was strong and irreversible, as indicated by the negligible removal of deposited bacteria with a high shear induced by passing an air bubble (Boks et al. 2008). The predicted individual trends for each surface and the difference between the top and bottom surfaces are close to observations except for one point at the highest shear rate (Figure 9). The agreement is then reasonably good, given the appreciable scatter of experimental points and the absence of any fitting parameter in the model.

Figure 10 illustrates how the model compares to the results of Roosjen et al. (2005) for the deposition of *Pseudomonas aeruginosa* on the bottom surfaces of a PFC made of native and PEO-modified glass. The simulation used density values of $1.1\,kg\,m^{-3}$ and an effective radius of the bacterium of $0.7\,\mu m$ (Roosjen et al. 2005). *P. aeruginosa* shows a much weaker attachment to glass *cf. S. epidermidis* and is more readily removed upon passing an air bubble (Boks et al. 2008). To address the weak attachment and capture the difference between the two surfaces Equation 7 was used as a boundary condition for Equation 2, K being an adjustable parameter. Given the crude model and the considerable scatter of the data, experimental points fall fairly reasonably within the range bounded by simulated results obtained for K values between 0.03 and 0.04 for unmodified glass and between 0.001 and 0.006 for PEO-modified surface (Figure 10). These K values appear reasonable; similar to the $K < 1$ expected for the weakly repulsive interaction of bacteria with glass and the $K \ll 1$ for the PEO-modified surface, known to be particularly repulsive to biomaterials.

Figures 9 and 10 also show that the simulations underestimate deposition on the bottom for small shear rates. One possible reason is that K could be affected by some unaccounted for near-surface hydrodynamic effects rendering K shear-rate-dependent. Indeed, Yiantsios and Karabelas (2003) obtained a good fit to experimental data using relations equivalent to K inversely proportional to σ or σ^{-2}, ie decreasing with shear rate, although no rationale for this dependence was given. Adopting such dependence here would still not explain the above discrepancy, since the predicted rate would drop more rapidly and make the deviation at high shear rates more

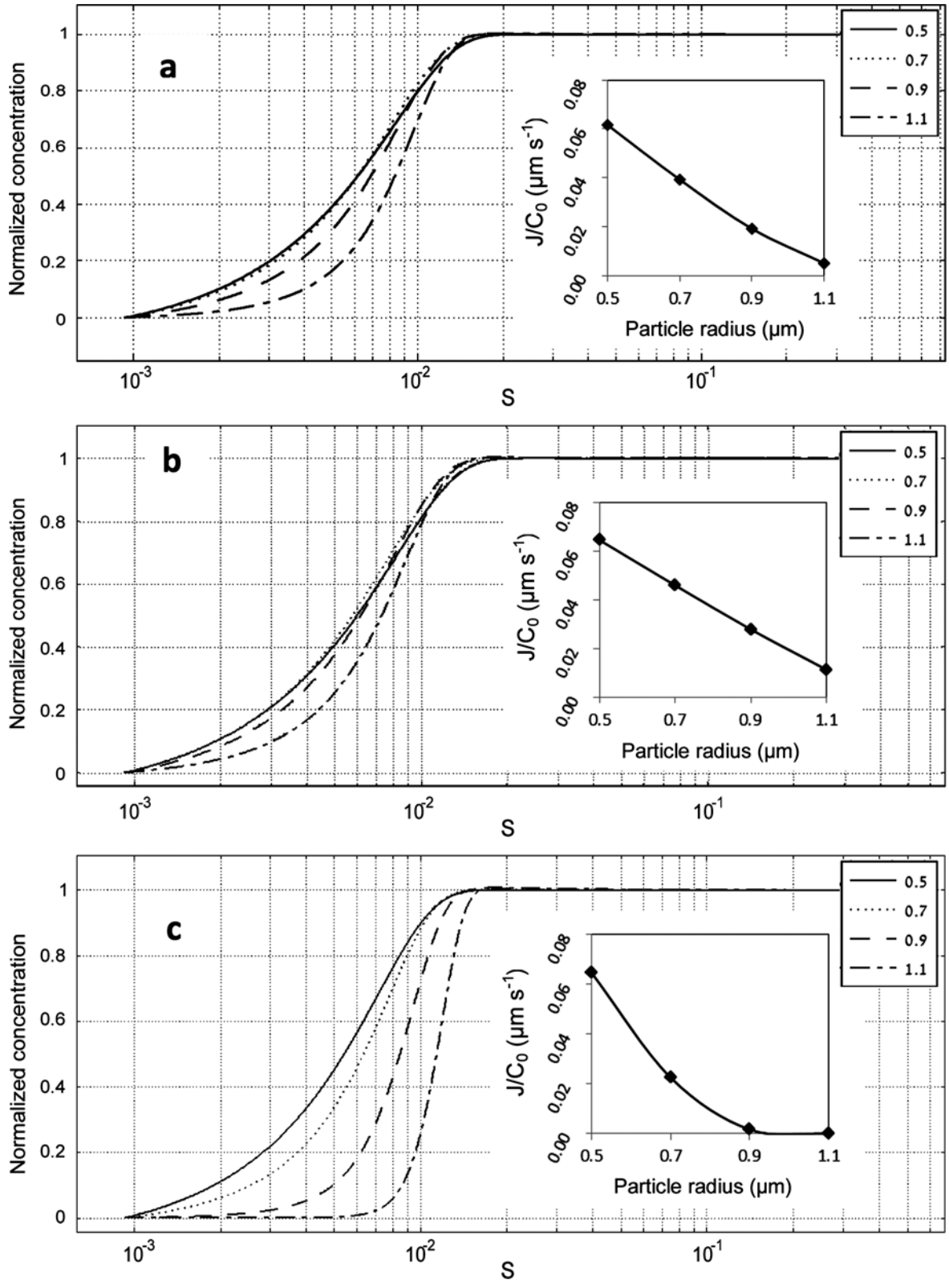

Figure 6. Calculated concentration profiles across the channel normalized to feed concentration for neutrally buoyant (a) particles and particle of density 1.1 g cm^{-3} depositing on the bottom (b) and top (c) walls for particle radii 0.5, 0.7, 0.9 and 1.1 μm. Wall shear rate of 800 s^{-1}.

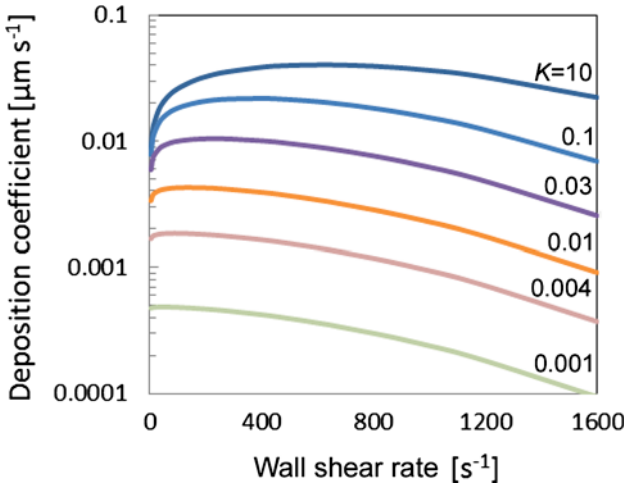

Figure 7. The calculated deposition rate for neutrally buoyant particles of radius 0.7 μm as a function of wall shear rate for different values of *K*.

pronounced. Neglecting the deviation at the highest shear rate, the present crude model with a constant *K* may then be fairly adequate and practically useful, as long as the shear rate range is not excessively wide.

The discrepancy could also be related to sedimentation. For instance, the actual density of bacteria could be underestimated, which may lead to the rate of deposition also being underestimated. This seems unlikely, since the density was already close to the maximum density reported for bacteria of 1.13 g cm^{-3} (Chen et al. 2009). Nevertheless, recent results (Li, Busscher, Norde, et al. 2011; Li, Busscher, van der Mei, et al. 2011) suggest another possibility, ie that adhered bacteria could be dragged and migrate downstream rather than stay at the same location, as for firmly adhered bacteria. It should be noted that the rate of deposition is usually determined from bacterial counts at a fixed location at several consecutive times. The 'apparent' deposition rate is then obtained from the slope *vs* time of the number density of bacteria per surface area normalized to the bulk density. However, this apparent deposition rate does not differentiate between the bacteria being deposited from the solution at the given location and those that have been deposited upstream and are migrating along the surface to that location. Compared to the actual deposition rate, ie the local flux of bacteria arriving from solution to the surface, which is computed in this study, the apparent rate may underestimate the actual deposition upstream and overestimate it downstream.

The apparent rate of deposition could have a somewhat different dependence on the flow rate, time, and distance from the inlet, *cf*. the actual rate of deposition. For instance, in the experiments of Li et al. (Li, Busscher, Norde, et al. 2011; Li, Busscher, van der Mei,

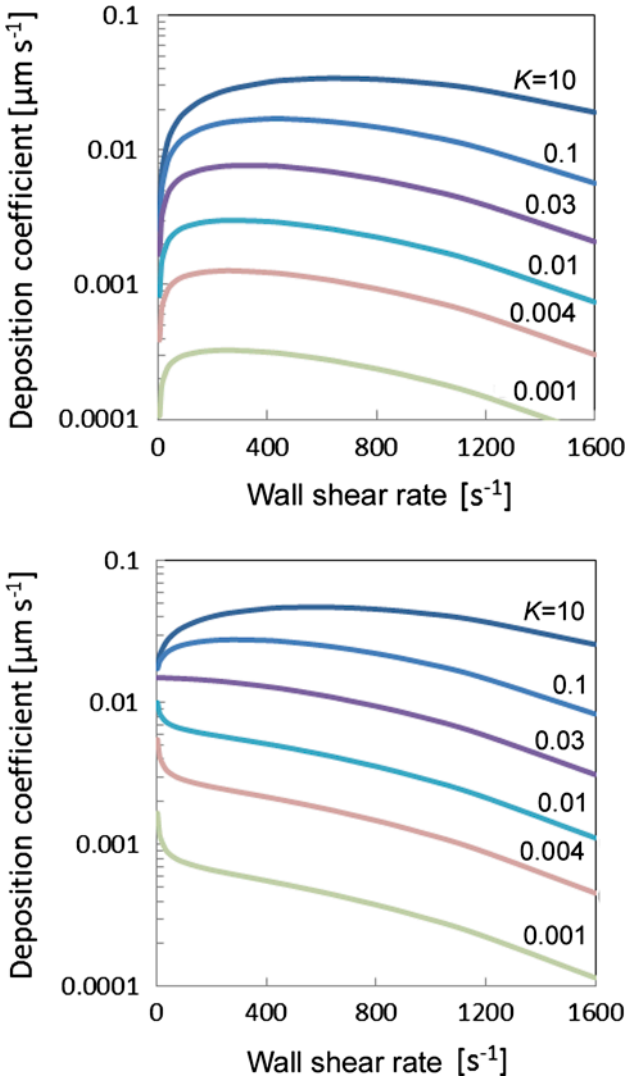

Figure 8. The deposition rate on the top (a) and bottom (b) wall as a function of wall shear rate for different values of *K*. The results were calculated for particles of radius 0.7 μm and density 1.1 g cm^{-3}.

et al. 2011) sedimentation was the dominant deposition mechanism and, without drag, would have yielded a density profile of deposited bacteria decreasing along the channel, in accord with the longitudinal variation of the deposition rate from the solution (Figure 3b). However, as a result of drag along the surface, the density of bacteria adhered to the bottom was redistributed and biased towards the outlet, the bias becoming more pronounced with time as more bacteria accumulated at the surface.

It may be challenging to separate the contributions from actual deposition from solution and from drag along the surface. In principle, for a given observation point it can be done by closing the balance of all the bacteria deposited from the inlet to the specified point over time. An alternative is to use an appropriate model. Clearly, drag along the surface is not included in the

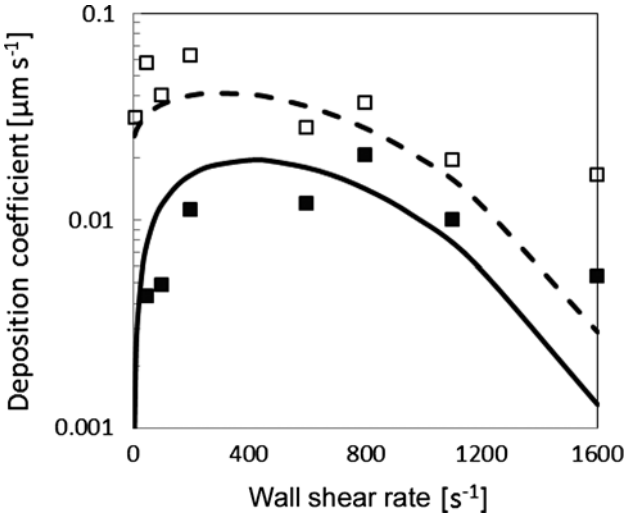

Figure 9. The normalized deposition rate of *S. epidermidis* ATCC 35983 on native glass surfaces. The symbols are experimental data of Boks et al. (2008) for the top (■) and bottom (□) walls of a PFC as a function of wall shear rate. The dashed and solid lines are model calculations of the top and bottom surfaces for particles of radius 0.9 μm and density 1.1 g cm^{-3} under perfect sink boundary conditions.

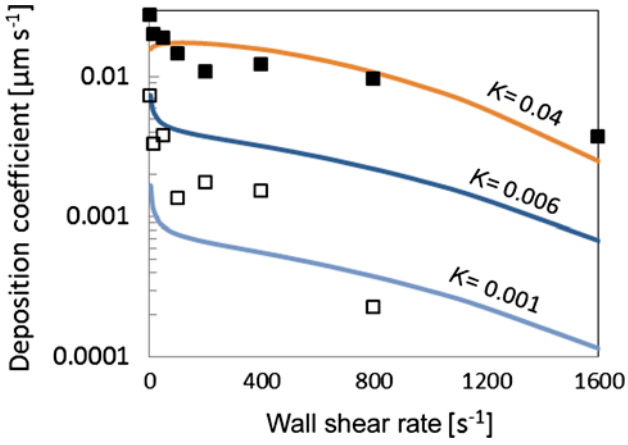

Figure 10. The normalized deposition rate of *P. aeruginosa* on native (■) and PEO-modified glass (□) surfaces forming the bottom of a PFC as a function of wall shear rate. The symbols are experimental data of Roosjen et al. (2005) and the solids lines are simulation results obtained for particles of radius 0.7 μm and density 1.1 g cm^{-3} under boundary condition given by Equation 7 with K values indicated.

present boundary condition, ie in Equation 7 with $C_s \approx 0$. Yet this may, in principle, be done by introducing a boundary condition with time- and position-dependent C_s and allowing a finite drag velocity of the bacteria along the surface. The drag velocity may be introduced in a phenomenological manner, similar to K, or calculated from the hydrodynamic drag force and the bacteria-surface friction coefficient. Weakly adhering bacteria (small K) are more likely to have low friction and be dragged more easily, even though, strictly speaking, adhesion and friction are not related directly (Israelachvili 2011). This is consistent with the fact that the present model shows better agreement for more strongly adhering bacteria (*cf.* Figures 9 and 10). Conversely, *S. aureus* used in the studies of Li and co-workers (Li, Busscher, Norde, et al. 2011; Li, Busscher, van der Mei, et al. 2011) shows a strong deposition on glass (Roosjen et al. 2003), yet the effect of drag still appeared to be of consequence for this system, indicating it may be of general importance.

In conclusion, for given fluid characteristics and channel geometry the dependence of the rate of bacterial deposition in a PFC on the wall shear rate may be simply and reasonably well described by Equations 2 and 7. These equations include convection, diffusion, sedimentation, lift, and bacteria-surface interaction using just three parameters: bacterial radius, buoyancy (density), and a dimensionless parameter K gauging the propensity of the particular system (bacteria and surface) to deposition. Future improvement may additionally incorporate a surface drag parameter, particularly for poorly adhering low-friction surfaces. Development of more accurate and, inevitably, more sophisticated hydrodynamic models of bacterial deposition could lead to more accurate relationships free of phenomenological parameters. Nevertheless, the present model may offer a reasonable compromise by including all the relevant physics with a minimal complexity and at a relatively low computational cost.

References

Adamczyk Z, Weronski P. 1999. Application of the DLVO theory for particle deposition problems. Adv Colloid Interface Sci. 83:137–226.

Altena FW, Belfort G. 1984. Lateral migration of spherical particles in porous flow channels: application to membrane filtration. Chem Eng Sci. 39:343–355.

Asmolov ES. 1999. The inertial lift on a spherical particle in a plane Poiseuille flow at large channel Reynolds number. J Fluid Mech. 381:63–87.

Bakker DP, Busscher HJ, van der Mei HC. 2002. Bacterial deposition in a parallel plate and a stagnation point flow chamber: microbial adhesion mechanisms depend on the mass transport conditions. Microbiology. 148:597–603.

Bjarnsholt T. 2011. Introduction to biofilms. In: Bjarnsholt T, Østrup PJ, Moser C, Høiby N, editors. Biofilm infections. New York (NY): Springer; p. 1–10.

Boks NP, Norde W, van der Mei HC, Busscher HJ. 2008. Forces involved in bacterial adhesion to hydrophilic and hydrophobic surfaces. Microbiology. 154:3122–3133.

Brenner H. 1961. The slow motion of a sphere through a viscous fluid towards a plane surface. Chem Eng Sci. 16:242–251.

Busscher HJ, van der Mei HC. 2006. Microbial adhesion in flow displacement systems. Clin Microbiol Rev. 19:127–141.

Camesano TA, Logan BE. 1998. Influence of fluid velocity and cell concentration on the transport of motile and nonmotile bacteria in porous media. Environ Sci Technol. 32:1699–1708.

Chen G, Hong Y, Walker SL. 2009. Colloidal and bacterial deposition: role of gravity. Langmuir. 26:314–319.

Cherukat P, Mclaughlin JB. 1994. The inertial lift on a rigid sphere in a linear shear flow field near a flat wall. J Fluid Mech. 263:1–18.

Costerton JW, Lewandowski Z, Caldwell DE, Korber DR, Lappin-Scott HM. 1995. Microbial biofilms. In: Ornston LN, Balows A, Greenberg EP, editors. Annual review of microbiology (Vol. 49). Palo Alto (CA): Annual Reviews; p. 711–745.

Cox R, Hsu S. 1977. The lateral migration of solid particles in a laminar flow near a plane. Int J Multiphase Flow. 3: 201–222.

de Kerchove AJ, Weronski P, Elimelech M. 2007. Adhesion of nonmotile *Pseudomonas aeruginosa* on 'soft' polyelectrolyte layer in a radial stagnation point flow system: measurements and model predictions. Langmuir. 23:12301–12308.

Di Carlo D. 2009. Inertial microfluidics. Lab Chip. 9:3038–3046.

Elimelech M. 1994. Particle deposition on ideal collectors from dilute flowing suspensions: mathematical formulation, numerical solution, and simulations. Sep Technol. 4:186–212.

Elimelech M, Gregory J, Jia X, Williams R. 1995. Particle deposition and aggregation. Oxford: BH.

Goldman A, Cox R, Brenner H. 1967. Slow viscous motion of a sphere parallel to a plane wall-I motion through a quiescent fluid. Chem Eng Sci. 22:637–651.

Gutman J, Walker SL, Freger V, Herzberg M. 2012. Bacterial attachment and viscoelasticity: physicochemical and motility effects analyzed with QCM-D. Environ Sci Technol. 47:398–404.

Haznedaroglu B, Zorlu O, Hill J, Walker S. 2010. Identifying the role of flagella in the transport of motile and nonmotile *Salmonella enterica* serovars. Environ Sci Technol. 44:4184–4190.

Ho BP, Leal LG. 1974. Inertial migration of rigid spheres in two-dimensional unidirectional flows. J Fluid Mech. 65:365–400.

Hoek E, Allred J, Knoell T, Jeong BH. 2008. Modeling the effects of fouling on full-scale reverse osmosis processes. J Membr Sci. 314:33–49.

Hoek EMV, Agarwal GK. 2006. Extended DLVO interactions between spherical particles and rough surfaces. J Colloid Interface Sci. 298:50–58.

Hogg AJ. 1994. The inertial migration of non-neutrally buoyant spherical particles in two-dimensional shear flows. J Fluid Mech. 272:285–318.

Hori K, Matsumoto S. 2010. Bacterial adhesion: from mechanism to control. Biochem Eng J. 48:424–434.

Israelachvili JN. 2011. Intermolecular and surface forces. Rev. 3rd ed. London: Academic Press.

Kalasin S, Santore M. 2008. Hydrodynamic crossover in dynamic microparticle adhesion on surfaces of controlled nanoscale heterogeneity. Langmuir. 24:4435–4438.

Kerchove AJ, Elimelech M. 2008. Bacterial swimming motility enhances cell deposition and surface coverage. Environ Sci Technol. 42:4371–4377.

Levich VG. 1962. Physicochemical hydrodynamics. Englewood Cliffs (NJ): Prentice-Hall.

Li J, Busscher HJ, Norde W, Sjollema J. 2011. Analysis of the contribution of sedimentation to bacterial mass transport in a parallel plate flow chamber. Colloids Surf, B. 84:76–81.

Li J, Busscher HJ, van der Mei HC, Norde W, Krom BP, Sjollema J. 2011. Analysis of the contribution of sedimentation to bacterial mass transport in a parallel plate flow chamber: part II: use of fluorescence imaging. Colloids Surf, B. 87:427–432.

Maniero R, Canu P. 2006. A model of fine particles deposition on smooth surfaces: I – theoretical basis and model development. Chem Eng Sci. 61:7626–7635.

Maniero R, Canu P. 2007. A model of fine particles deposition on smooth surfaces: II – comparison with experimental data and simplified models. Chem Eng Sci. 62:2821–2832.

Matas JP, Morris JF, Guazzelli E. 2004. Inertial migration of rigid spherical particles in Poiseuille flow. J Fluid Mech. 515:171–195.

Palmer RJ, White DC. 1997. Developmental biology of biofilms: implications for treatment and control. Trends Microbiol. 5:435–440.

Palumbo AV, Ferguson RL, Rublee PA. 1984. Size of suspended bacterial cells and association of heterotrophic activity with size fractions of particles in estuarine and coastal waters. Appl Environ Microbiol. 48:157–164.

Ploux L, Ponche A, Anselme K. 2010. Bacteria/material interfaces: role of the material and cell wall properties. J Adhes Sci Technol. 24:2165–2201.

Prescott LM, Harley JP, Klein DA, editors. 2002. Microbiology, 5th ed. Boston (MA): McGraw-Hill.

Roosjen A, Boks NP, van der Mei HC, Busscher HJ, Norde W. 2005. Influence of shear on microbial adhesion to PEO-brushes and glass by convective-diffusion and sedimentation in a parallel plate flow chamber. Colloids Surf, B. 46:1–6.

Roosjen A, Kaper HJ, van der Mei HC, Norde W, Busscher HJ. 2003. Inhibition of adhesion of yeasts and bacteria by poly(ethylene oxide)-brushes on glass in a parallel plate flow chamber. Microbiology. 149:3239–3246.

Saffman PG. 1965. The lift on a small sphere in a slow shear flow. J Fluid Mech. 22:385–400.

Segre G, Silberberg A. 1962. Behavior of macroscopic rigid spheres in Poiseuille flow. J Fluid Mech. 14:136–157.

Song L, Elimelech M. 1995. Particle deposition onto a permeable surface in laminar flow. J Colloid Interface Sci. 173:165–180.

van Loosdrecht MCM, Lyklema J, Norde W, Zehnder AJB. 1989. Bacterial adhesion: a physicochemical approach. Microb Ecol. 17:1–15.

van Oss CJ. 2006. Interfacial forces in aqueous media, 2nd ed. Boca Raton (FL): Taylor & Francis.

Vasseur P, Cox R. 1976. The lateral migration of a spherical particle in two-dimensional shear flows. J Fluid Mech. 78:385–413.

Wang H, Sodagari M, Chen Y, He X, Newby BZ, Ju LK. 2011. Initial bacterial attachment in slow flowing systems: effects of cell and substrate surface properties. Colloids Surf, B. 87:415–422.

Wyatt PJ, Phillips DT. 1972. Structure of single bacteria from light scattering. J Theor Biol. 37:493–501.

Yahiaoui S, Feuillebois F. 2010. Lift on a sphere moving near a wall in a parabolic flow. J Fluid Mech. 662:447–474.

Yiantsios SG, Karabelas AJ. 2003. Deposition of micron-sized particles on flat surfaces: effects of hydrodynamic and physicochemical conditions on particle attachment efficiency. Chem Eng Sci. 58:3105–3113.